ACS APPLIED MATERIALS & INTERFACES

Research Article

www.acsami.org

Ultrasensitive Hydrogen Sensor Based on Pt-Decorated WO_3 Nanorods Prepared by Glancing-Angle dc Magnetron Sputtering

M. Horprathum,*[,†] T. Srichaiyaperk,[‡] B. Samransuksamer,[§] A. Wisitsoraat,[∥] P. Eiamchai,[†] S. Limwichean,[†] C. Chananonnawathorn,[‡] K. Aiempanakit,[‡] N. Nuntawong,[†] V. Patthanasettakul,[†] C. Oros,[⊥] S. Porntheeraphat,[#] P. Songsiriritthigul,[▽] H. Nakajima,[○] A. Tuantranont,[∥] and P. Chindaudom[†]

[†]Optical Thin-Film Laboratory, National Electronics and Computer Technology Center, Pathumthani 12120, Thailand

[‡]Department of Physics, Faculty of Science and Technology, Thammasat University, Pathumthani, 12121 Thailand

[§]Department of Physics, Faculty of Science, King Mongkut's University of Technology Thonburi, Bangkok, 10140, Thailand

[∥]Nanoelectronics and MEMS Laboratory, National Electronics and Computer Technology Center, Pathumthani 12120, Thailand

[⊥]Faculty of Liberal-arts, Rajamangala University of Technology Rattanakosin, Nakornpathom 73170, Thailand

[#]Photonic Technology Laboratory, National Electronics and Computer Technology Center, Pathumthani 12120, Thailand

[▽]NANOTEC-SUT Center of Excellence on Advanced Functional Nanomaterials and School of Physics, Suranaree University of Technology, Nakhon Ratchasima 30000, Thailand

[○]Synchrotron Light Research Institute, Maung, Nakhon Ratchasima 30000, Thailand

ABSTRACT: In this work, we report an ultrasensitive hydrogen (H_2) sensor based on tungsten trioxide (WO_3) nanorods decorated with platinum (Pt) nanoparticles. WO_3 nanorods were fabricated by dc magnetron sputtering with a glancing angle deposition (GLAD) technique, and decorations of Pt nanoparticles were performed by normal dc sputtering on WO_3 nanorods with varying deposition time from 2.5 to 15 s. Crystal structures, morphologies, and chemical information on Pt-decorated WO_3 nanorods were characterized by grazing-incident X-ray diffraction, field-emission scanning electron microscopy, energy-dispersive X-ray spectroscopy, and photoelectron spectroscopy, respectively. The effect of the Pt nanoparticles on the H_2-sensing performance of WO_3 nanorods was investigated over a low concentration range of 150−3000 ppm of H_2 at 150−350 °C working temperatures. The results showed that the H_2 response greatly increased with increasing Pt-deposition time up to 10 s but then substantially deteriorated as the deposition time increased further. The optimally decorated Pt−WO_3 nanorod sensor exhibited an ultrahigh H_2 response from 1530 and 214 000 to 150 and 3000 ppm of H_2, respectively, at 200 °C. The outstanding gas-sensing properties may be attributed to the excellent dispersion of fine Pt nanoparticles on WO_3 nanorods having a very large effective surface area, leading to highly effective spillover of molecular hydrogen through Pt nanoparticles onto the WO_3 nanorod surface.

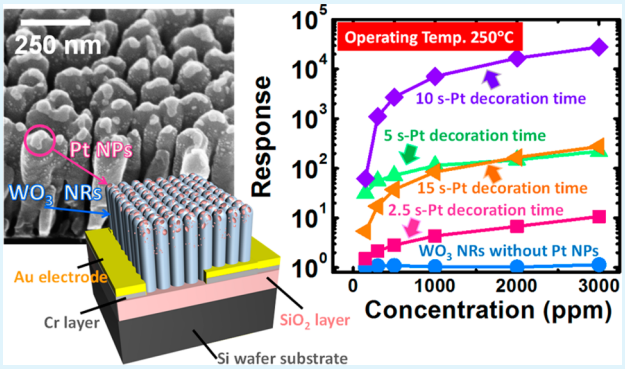

KEYWORDS: *tungsten trioxide nanorods, glancing-angle deposition, Pt nanoparticles, H_2 sensor, sputtering*

INTRODUCTION

Hydrogen (H_2) is a potential clean energy source and important raw material for chemical, semiconductor, and many other industries. However, it is extremely flammable, highly explosive, and difficult to store due to high leaking susceptibility. Additionally, it cannot be detected by human beings because it is colorless and odorless.[1] Increasing use of H_2 has continuously led to a very high demand of highly sensitive and reliable sensors to detect low concentrations of H_2 in order to meet safety requirements. Over the past several years, various metal oxide semiconductor (MOS) sensors have been extensively studied and used for hydrogen detection because of the simplicity, reliability, cost-effectiveness, and mass-production availability.[2−7] Their sensing principle is based on the change of the electrical conductivity of the MOS material due to chemisorptions and catalytic reactions of gas-phase species on the material surface. Thus, the performance of MOS gas sensors is directly dependent on the type of MOS materials as well as their surface morphology. Among various MOS materials, tungsten oxide (WO_3), an n-type semiconductor with a band gap of 2.6−3.6 eV,[8] exhibits particularly promising gas-sensing performance toward some specific target gases

Received: August 11, 2014
Accepted: November 25, 2014
Published: November 25, 2014

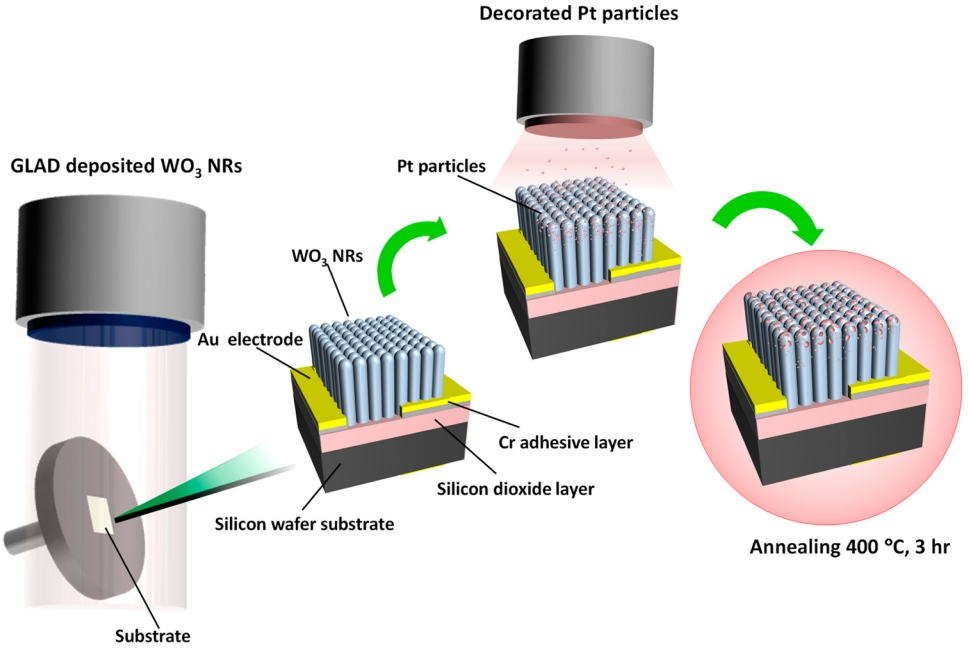

Figure 1. Schematic of the Pt-decorated WO_3 nanorod array fabricated by the glancing-angle dc magnetron sputtering deposition.

including NO_2,[9,10] O_3,[11] NH_3,[12] and H_2.[13] In addition, WO_3 can be practically produced in several nanostructural forms, including nanowires, nanorods, nanotubes, and nanobelts. Gas sensors based on WO_3 nanostructures have demonstrated high sensitivity, fast response, and high reproducibility due to their large surface-to-volume ratio, high crystallinity, and good stability.[9,10,12]

WO_3 nanostructures can be prepared by several techniques including thermal oxidization,[14] flame spray pyrolysis,[15] chemical vapor deposition (CVD),[16] physical vapor deposition (PVD),[17,18] and hydrothermal or other chemical-route syntheses. Many of these methods entail complex procedures for deposition or functionalization using solution-based processing, and some of them require high-temperature treatments that produce nanostructures with random size, distribution, and orientation. Such methods are not reliable for practical applications due to poor reproducibility. Thus, means to construct well-ordered nanostructures are highly preferred. The general approach for fabrication of ordered nanostructures is based on micro/nanoelectronic fabrication processes involving e-beam lithography, nanolithography, and reactive ion etching, which require expensive instrumentation or complicated fabrication procedures and are not suitable for low-cost gas-sensing applications. A glancing-angle deposition (GLAD) technique based on the PVD process has recently emerged as a promising cost-effective alternative that can fabricate a variety of well-ordered nanostructures, i.e., aligned nanorods, nanoblades, and zigzag nanocolumns.[19,20] GLAD modifies the standard PVD by tilting the substrate surface to an angle of less than 10° with respect to the direction of vapor flux. The size, shape, and porosity of nanostructures produced by GLAD can be very well controlled by the angle of incidence and optional substrate rotation.

Recently, we reported thin film gas sensors based on vertically aligned WO_3 nanorods prepared by the GLAD technique and demonstrated its promising NO_2 and ethanol gas-sensing responses.[9,10] Nevertheless, the gas-sensing performance of aligned WO_3 nanorods should be further improved for other gas-sensing applications by properly incorporating effective additives. In particular, platinum (Pt) is reported to be one of the most active noble metal catalysts that can greatly enhance H_2-sensing response of semiconducting metal oxide thin films and nanoparticles.[21−29] However, there is no report of its combination with WO_3 nanorods prepared by GLAD for gas sensing. In this work, WO_3 nanorods made by the GLAD technique are decorated with Pt nanoparticles by precisely controlled dc sputtering and the influences of Pt nanoparticulate density on crystal structures, surface morphologies, and H_2-sensing performances are systematically investigated.

2. EXPERIMENTAL DETAILS

2.1. Fabrication of WO_3 and Pt−WO_3 Nanorods Gas Sensors.

The fabrication process of Pt−WO_3 nanorod sensors is demonstrated in Figure 1. Gas sensors were produced by direct deposition of sensing films on SiO_2/Si substrates with interdigital gold (Au) electrodes, which were used to reduce the resistance of highly resistive WO_3 material. Electrodes were fabricated by consecutive sputtering of ∼50 nm Cr and ∼300 nm Au films on a 1 μm thick SiO_2/Si wafer with a prepatterned photoresist layer followed by a standard photoresist lift-off procedure. The interdigital spacing and active electrode area were ∼100 μm and ∼2 × 5 mm^2, respectively. Additionally, bare silicon wafers were used as substrates for structural and morphological characterization. Substrates were successively sonicated in deionized water, acetone, and isopropanol followed by drying in nitrogen before loading into the sputtering chamber.

After pumping down to a base pressure of 5.0×10^{-6} mbar, WO_3 nanorod structures were deposited onto the substrates by reactive dc magnetron sputtering with GLAD. The magnetron was home built with a diameter of 3 in. and an average magnetic field of 50 mT above the erosion track. A 3 in. diameter tungsten disc with 99.995% purity (K. J. Lesker) was used as the sputtering target and presputtered at a 50 W dc power in an argon atmosphere at 3×10^{-3} mbar in order to remove surface contamination on the target. The substrate was located 70 mm away from the target, tilted at 85° with respect to the vapor incident flux (the vertical axis) and rotated at a speed of 1.6 rpm. Reactive sputtering of WO_3 was then performed without substrate heating in a mixture of 99.999% argon and 99.999% oxygen supplied through mass-flow controllers (MKS) at constant flow rates of 8 and 24 sccm, respectively. The dc bias, dc power, operating pressure, and

deposition time for WO_3 sputtering were 580 V, 175 W, 5×10^{-3} mbar, and 60 min, respectively. The substrate temperature monitored with a temperature sensor attached on the substrate holder was found to increase from 30 to 95 °C by plasma-induced heating. Subsequently, Pt catalyst nanoparticles were decorated onto a set of WO_3 nanorod samples by normal dc magnetron sputtering in an Ar atmosphere without substrate heating. The dc bias, dc power, Ar flow rate, deposition pressure, and substrate temperature for Pt sputtering were 400 V, 40 W, 10 sccm, 3×10^{-3} mbar, and 30 °C, respectively. The Pt deposition time was varied from 2.5 to 15 s in order to control the density of Pt nanoparticles. Finally, all prepared samples were annealed in air at 400 °C for 3 h in order to stabilize the WO_3 nanorod structure.

2.2. Structural and Gas-Sensing Characterization. Crystal structures of WO_3 and Pt–WO_3 nanorods were characterized by glancing incident X-ray diffraction (GIXRD; Rigaku) using a Cu Kα radiation. XRD measurement was conducted at a scanning speed of 3°/min and a 2θ step of 0.02° using an X-ray source operated at an applied voltage and a current of 50 kV and 300 mA, respectively. The morphologies and chemical compositions of all samples were examined by field emission-scanning electron microscopy (FE-SEM; Hitachi SU8030) and energy-dispersive X-ray spectrometry (EDS). Surface elemental composition and oxidation states of sensing films were evaluated by photoelectron spectroscopy (PES) using a VG Scientific CLAM2 energy analyzer with a synchrotron light source at the PES beamline of the Synchrotron Light Research Institute of Thailand.[30]

H_2 gas-sensing properties of undecorated and Pt-decorated WO_3 nanorods were measured using the standard flow-through method under a controlled atmosphere in a stainless steel chamber. A constant flux of synthetic air of 2 L/min as gas carrier was mixed with the desired concentration of H_2 pollutant dispersed in synthetic air. Gas flow rates were precisely manipulated using a computer-controlled multichannel mass-flow controller (Brook Instruments). The electrical resistance of sensors was acquired and continuously monitored using a picoammeter (KEITHLEY 6487) controlled by a personal computer with LabView-based software. The resistance between the two electrodes was measured at an applied voltage of 0.1 V and different operating temperatures ranging from 150 to 350 °C as a function of H_2 concentration in the range of 150–3000 ppm. The gas-sensing response to H_2 was estimated according to the standard definition of reducing gas, $S = R_a/R_g$, where R_a and R_g are the stable electrical resistance before and after H_2 exposure, respectively. The response definition was reversed for oxidizing gas (i.e., NO_2). In addition, response and recovery times were calculated from the time required to reach 90% of the response signal and the time needed to recover 90% of the original baseline signal, respectively.

3. RESULTS AND DISCUSSION

3.1. Structural Analysis. The GIXRD patterns of annealed undecorated and Pt-decorated WO_3 nanorods with different Pt decoration times are shown in Figure 2. It is seen that undecorated and all Pt-decorated WO_3 nanorods have similar polycrystalline structure that is well matched to monoclinic phase WO_3 (JCPDS 43-1035). In addition, Pt decoration has an insignificant influence on the preferred crystallographic orientation of WO_3 nanorods, and there is no diffraction peak corresponding to the Pt phase of decorated nanoparticles. The result is expected since Pt nanoparticulate films should be very thin, so that its diffraction signal is too low to be detected by a standard X-ray diffractometer. EDS and FE-SEM will be used to confirm the presence of Pt nanoparticles.

Figure 3a–e shows SEM images of WO_3 nanorods with various Pt decoration times. It can be seen that all samples comprise similarly uniform and high-density vertically aligned columnar nanorods with length and diameter in the ranges of ~400–450 and 80–100 nm, respectively. WO_3 nanorods

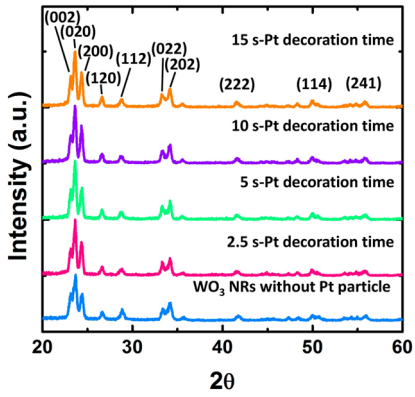

Figure 2. GIXRD patterns of the WO_3 and Pt-decorated WO_3 nanorod arrays.

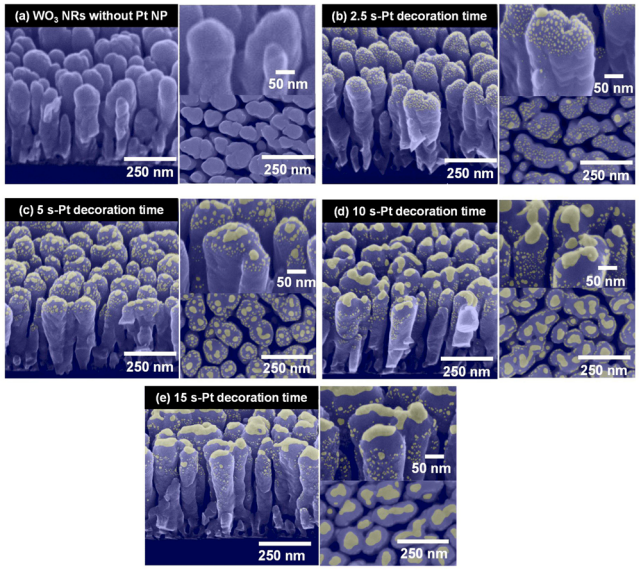

Figure 3. SEM images of WO_3 nanorod films with a Pt decoration time of (a) 0 (undecorated), (b) 2.5, (c) 5, (d) 10, and (e) 15 s.

(Figure 3a) are formed by atomic self-shadowing due to glancing angle deposition and limited adatom diffusion mechanisms described elsewhere.[19,20,31,32] After 2.5 s Pt decoration (Figure 3b) a number of small bright spots are observed to be distributed rather uniformly over the nanorods. They are expected to be Pt nanoparticles decorated on WO_3 nanorods since such bright nanodots were not observed on undecorated samples. In addition, it can be noticed that the nanoparticles are mostly located near the top of nanorods, and the particle diameter is estimated be in the range of ~3–5 nm. As the Pt decoration time increases to 5 s, the particle diameter especially on the top regions increases to ~5–10 nm and more nanoparticles are seen down below the top end. When the Pt decoration time is further increased to 10 s, the particle diameter especially on the top regions increases further to ~8–30 nm and nanoparticles are seen to penetrate almost half way to the bottom. Moreover, the top particles are slightly agglomerated with adjacent ones. At the longest Pt decoration time of 15 s the particles particularly in the top area are highly agglomerated into connected islands and go in more than half way to the bottom.

To understand formation of Pt nanoparticles on WO_3 nanorods, Pt-decorated WO_3 nanorods were also examined

by SEM before and after annealing. Before annealing it was found that isolated nanoparticles were initially formed and turned into interconnected islands with increasing deposition time. At the initial deposition stage Pt atoms formed individual isolated islands to minimize the surface free energy and then grew into larger Pt islands according to the Volmer–Weber mechanism for nonwetting surfaces as depicted in Figure 1.[33] After the annealing treatment at 400 °C for 3 h, Pt islands and clusters were transformed into the nanoparticles due to the wetting phenomenon (see also the rightmost drawing in Figure 1), which could occur at relatively low temperature because very thin metal film exhibited a much lower melting point and higher surface tension than its bulk form.[34,35] The increasing size of islands with increasing Pt decoration time should be due to the fact that the sizes of annealed Pt nanoparticles accordingly follow those of initial Pt islands formed after Pt sputtering, which are increased with increasing sputtering time.

The presence of the Pt element on WO_3 nanorods was successfully confirmed from EDS spectra of undecorated and Pt-decorated WO_3 nanorods as illustrated in Figure 4a and 4b,

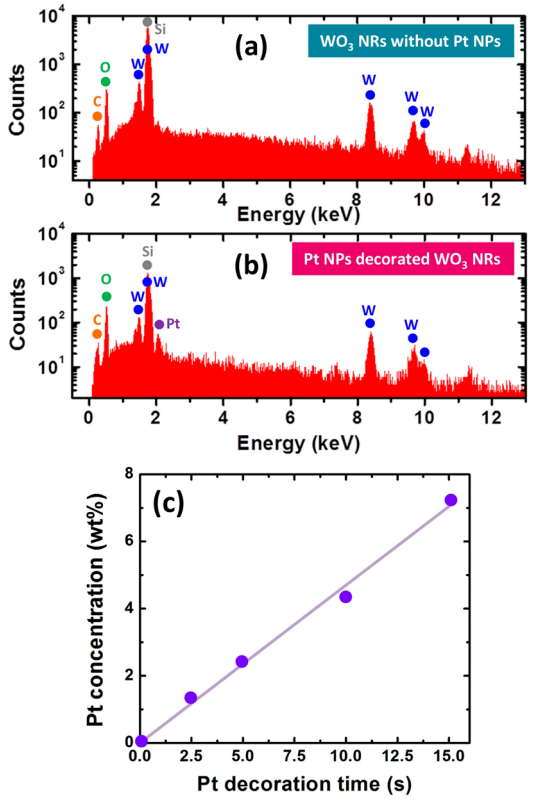

Figure 4. Typical EDX spectra of (a) undecorated and (b) 10s-Pt-decorated WO_3 nanorods. (c) Calculated weight percentage of Pt from EDX data as a function of Pt decoration time.

respectively. In addition, carbon contamination is observed. For the main W element it is seen that the main W M_β peak is overlapped with the Si K peak of substrate, so the presence of W atoms must be confirmed from the occurrence of minor peaks in W series. The weight percentage of the Pt element relative to all elements in WO_3 nanorod films was estimated from the EDS spectrum and plotted as a function of Pt decoration time as shown in Figure 4c. It can be seen that the Pt concentration on the WO_3 nanorod film increases linearly from 1.3 to 7.6 wt % as Pt decoration time increases from 2.5 to 15 s, confirming a constant deposition rate of Pt material.

The presence of Pt on WO_3 nanorods was further confirmed by PES survey spectra as illustrated in Figure 5. The spectra

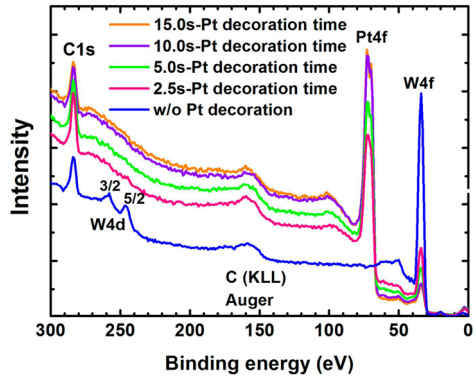

Figure 5. PES survey spectra of WO_3 nanorod films with different Pt decoration times taken at photon energy of 420 eV.

show expected elements of the materials and typical surface carbon contamination. In addition, the intensity of the Pt 4f peak tends to increase, while the heights for the W 4f–W 4d peaks decrease correspondingly with increasing Pt decoration time in accordance with an expected increase in Pt contribution. It should be noted that surface ion sputtering typically used to avoid C 1s photoelectron and C (KLL) Auger electron peaks was not applied before all measurements because Pt nanoparticles could also be partially removed, significantly affecting the compositions of surfaces.

The state of the Pt element of Pt-decorated samples with different Pt decoration times was further evaluated by PES fine scan of the Pt 4f peak with 120 eV photon energy as shown in Figure 6a. The Pt 4f doublet peaks can be deconvoluted with Shirley background subtraction into three Gaussian doublet peaks as illustrated in Figure 6b. The Pt $4f_{7/2}$ peaks at 72.0, 73.1, and 74.2 eV along with their corresponding Pt $4f_{5/2}$ pairs at 75.1, 76.2, and 77.4 eV can be ascribed to Pt^0, Pt^{2+}, and Pt^{4+} species, respectively.[36,37] Pt^0, unoxidized Pt species, are expected to locate at the inner surface of Pt nanoparticles, while Pt^{2+} can be associated with physisorbed PtO formed at the very top layer of the Pt surface, and Pt^{4+}, the fully oxidized Pt species, may be created by chemical coordination at the Pt–WO_3 interface.

The relative percentages of different Pt species are calculated and plotted with Pt decoration time as shown in Figure 6c. It is seen that the contribution of Pt^0 linearly increases while that of Pt^{2+} is almost constant and that of Pt^{4+} decreases steadily with increasing Pt decoration time from 2 to 15 s. The results may be explained based on the observed SEM results that the size of Pt nanoparticles tends to increase with increasing Pt decoration time, leading to reduction of boundaries of Pt–WO_3 interface and less Pt^{4+} species observable by PES. Figure 6c also shows the atomic percentage of the Pt relative to the combined Pt and W atoms on the surface detected by the PES technique. It is seen that the percentage of the surface Pt atoms increases with decreasing rate as the Pt decoration time increases from 2.5 to 10 s and becomes almost insensitive to Pt decoration time in the range of 10–15 s. The result is in contrast to the EDS data in Figure 4c. A possible explanation for this anomaly is that a larger portion of Pt may penetrate deeper into the lower part of

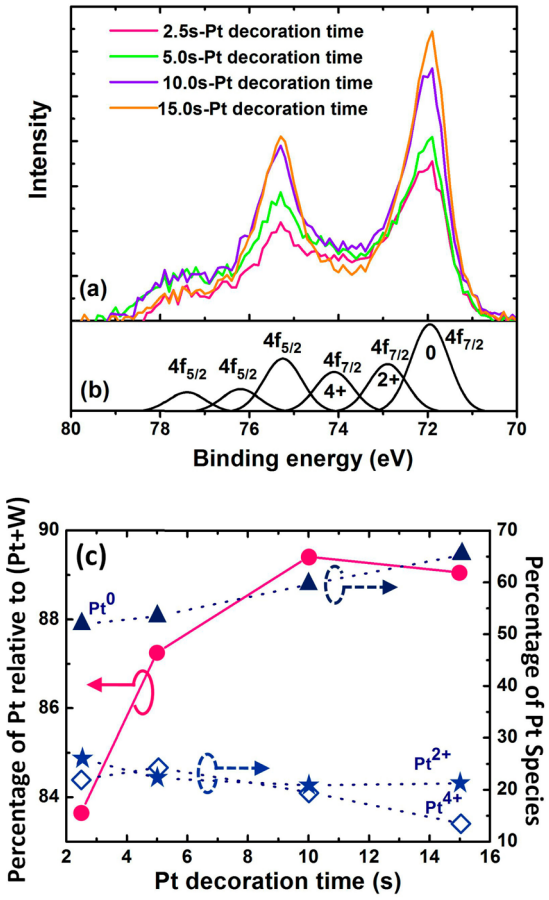

Figure 6. (a) Pt-4f PES spectra of WO_3 nanorod films with different Pt decoration times taken at a photon energy of 120 eV, (b) typical deconvoluted Pt $4f_{7/2}$ and $4f_{5/2}$ peaks, and (c) integrated Pt peak area and percentages of Pt species vs Pt decoration time.

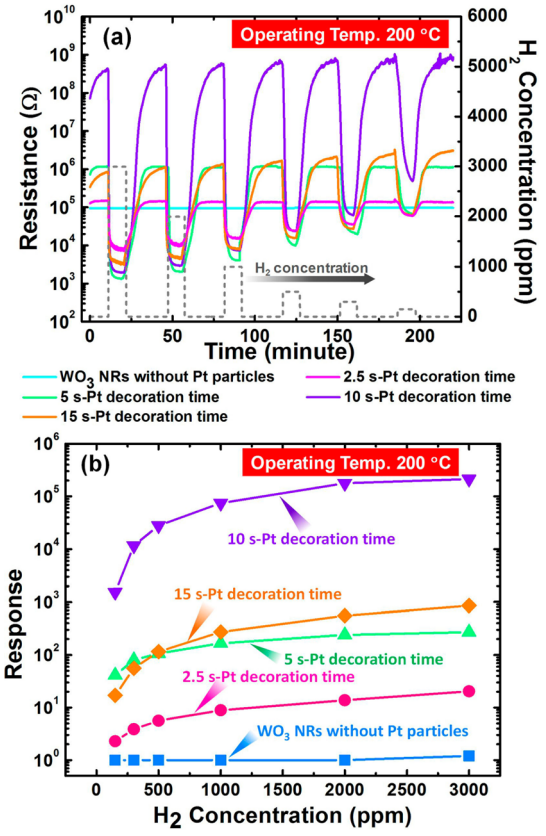

Figure 7. (a) Change in resistance and (b) gas response of WO_3 nanorods with different Pt decoration times toward 100−3000 ppm of H_2 at the optimal operating temperature of 200 °C.

WO_3 nanorods as more Pt atoms are accumulated over long Pt decoration time as observed from SEM images in Figure 3. The deeper Pt atoms cannot be seen by the PES technique, leading to a limited percentage of Pt on the surface, which is in contrast to the increasing percentage of Pt atoms detected by EDS through the film.

3.2. Gas-Sensing Properties. The H_2-sensing characteristics of the WO_3 nanorods and Pt-decorated WO_3 nanorods with different Pt decoration times were investigated. Figure 7a shows the change in resistance of the undecorated and Pt-decorated WO_3 nanorods under exposure to H_2 pulses with concentrations ranging from 150 to 3000 ppm at 200 °C operating temperature. It is evident that undecorated WO_3 nanorods exhibited almost no resistance change under H_2 exposure at 200 °C, consistent with previously published literature.[24−26] With the decoration of the Pt nanoparticles, the resistance changes substantially upon H_2 introduction and the magnitudes of resistance change depend considerably on Pt decoration time and gas concentration. In particular, 10s-Pt-decorated WO_3 nanorods exhibits the largest resistance changes of more than 5 orders of magnitude at 1000−3000 ppm of H_2 concentrations. Thus, the decoration of Pt nanoparticles greatly enhances the H_2-sensing performances of WO_3 nanorods. In addition, it can be noticed that the large resistance change is correspondingly accompanied by the large increase of baseline resistance of Pt-decorated WO_3 sensors. The baseline resistance significantly increases from $\sim 10^5$ to $\sim 5 \times 10^8$ Ω as the Pt decoration time increases from 0 to 10 s. However, it is reduced to $\sim 10^6$ Ω when the Pt decoration time increases further to 15 s.

The corresponding gas-sensing response calculated from the change in resistance of undecorated and Pt-decorated WO_3 nanorods are plotted as a function of H_2 concentration as shown in Figure 7b. It is seen that the response substantially increases by about 1 and 2 orders of magnitude with Pt decoration times of 2.5 and 5 s, respectively. As the Pt decoration time increases to 10 s, the response very sharply increases by 5 orders of magnitude. However, the response increment relative to the undecorated one is reduced to around 3 orders of magnitude when the Pt decoration time increases further to 15 s. Thus, the Pt decoration time of 10 s represents an optimal decoration condition for enhancing H_2-sensing response of WO_3 nanorods. The optimally decorated WO_3 nanorods exhibits an exceptionally high response of 2.2×10^5 to 3000 ppm of H_2 at a relatively low operating temperature of 200 °C. Moreover, the response is seen to increase rather slowly with increasing H_2 concentration, and the values are still substantial even at low concentrations of 150−500 ppm. The response curves are found to follow the well-known power law. After fitting the response curve with the power law, the detection limit of the optimal sensor where the response reaches 1.1 (10% resistance change) is estimated to be around 0.5 ppm, which is much lower than most previous reports in the literature.[21−28]

The operating temperature generally has a significant influence on gas adsorption/desorption and gas-sensing characteristics of metal oxide gas sensors. The effect of

dx.doi.org/10.1021/am505127g | ACS Appl. Mater. Interfaces 2014, 6, 22051−22060

operating temperature on the gas-sensing response and response/recovery time at 3000 ppm of H_2 concentration of the optimal Pt-decorated WO_3 nanorods is demonstrated in Figure 8a and 8b, respectively. It is seen that the sensors exhibit

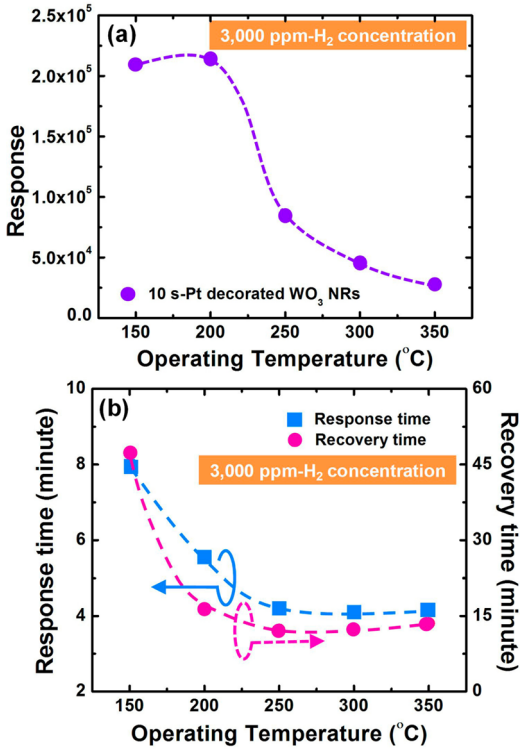

Figure 8. (a) Gas response and (b) response/recovery times versus operating temperature of 10 s-Pt-decorated WO_3 nanorod-sensing film toward 3000 ppm of H_2.

similarly high hydrogen response at low operating temperature (150−200 °C), and the response monotonically and substantially decreases with increasing operating temperature up to 350 °C. On the other hand, the response and recovery times tend to decrease with increasing operating temperature. In particular, the response and recovery times considerably increase at the lowest operating temperature of 150 °C. Thus, the optimal operating temperature that yields high sensor response with satisfactory response and recovery times is 200 °C. These observations are consistent with many other reports in the literature.[22−28]

The selectivity of the Pt-decorated WO_3 sensors has been evaluated for H_2, H_2S, NH_3, NO_2, C_2H_2, SO_2, and CO at their critical concentrations and operating temperature of 200 °C as shown in Figure 9. It is seen that the hydrogen selectivity of WO_3 nanorod sensors is significantly dependent on Pt decoration time. Without Pt decoration (Pt decoration time = 0 s), WO_3 nanorods exhibit high responses to NO_2, H_2S, C_2H_2, and NH_3 but low responses to H_2, SO_2, and CO. With the lowest Pt decoration time of 2.5 s, H_2 response increases considerably and is comparable with those of NO_2, H_2S, and NH_3, while the response to C_2H_2 becomes relatively low, and the responses to SO_2 and CO remain very low. As the decoration time increases to 5 s, H_2 response turns out to be the highest as the responses to H_2S, C_2H_2, and NH_3 are still high while NO_2 response becomes low and comparable with SO_2 response. As the Pt decoration time further increases to 10 s, H_2 response increases greatly while H_2S response remains

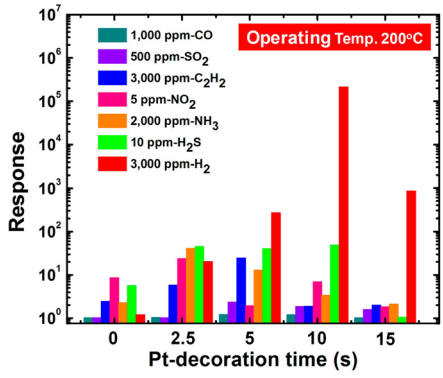

Figure 9. Selectivity histograms for H_2, H_2S, NH_3, NO_2, C_2H_2, SO_2, and CO at their critical concentrations of WO_3 nanorods with different Pt decoration times at the optimal operating temperature of 200 °C.

about the same and responses to all other gases decrease. At the longest Pt decoration time, response to H_2 decreases by more than 2 orders of magnitude and those to most other gases also reduce substantially. The results indicate that the H_2 selectivity of a WO_3 nanorod sensor can be greatly improved by decoration with high concentrations of Pt nanoparticles, which is in agreement with many other reports of Pt/WO_3 sensors prepared by different methods.[22−28] In addition to its promising performance, Pt-decorated aligned WO_3 nanorod sensors can offer better reproducibility and stability than many other methods because of its very well-controlled fabrication process.

Stability, repeatability, and reproducibility are other critical characteristics of gas sensors to be used in commercial applications. The optimally decorated WO_3 nanorods were tested over a large number of sensing cycles at various operating temperatures for 2 months. The results showed that the sensor exhibited good repeatability with less than 10% of response variation upon 100 repeated test cycles at 3000 ppm of H_2 and 200 °C. In addition, it showed a small drift in response and resistance of less than 15% after 2 months of operation. Moreover, the fabrication process offers good reproducibility with a response variation of less than 20% from 10 sensors fabricated from the same batch. The excellent stability, repeatability, and reproducibility can be attributed to the high structural as well as material stability of WO_3 nanorods decorated with Pt nanoparticles and the high reproducibility of sputtering and GLAD processes.

3.3. Gas-Sensing Mechanisms. From the results, undecorated WO_3 nanorods exhibit almost no response to H_2 at operating temperatures up to 300 °C, and Pt decoration leads to a dramatic enhancement of H_2 response. This is in agreement with many reports on Pt-loaded WO_3 materials prepared by different methods.[22−28] The results will be explained based on physical models of WO_3 nanorods with different Pt decorations as demonstrated in Figure 10. For undecorated WO_3 nanorods (Figure 10a), hydrogen sensing relies on direct reduction of H_2 with chemisorbed oxygen species (i.e., O^-, O^{2-}, and O_2^-) on n-type semiconducting WO_3 surface, which is reported to have a very low reaction rate at temperatures below 400 °C.[18] With the presence of Pt, the H_2 reduction rate will be greatly enhanced by chemical sensitization of Pt via a spillover effect.[22−28] For Pt on WO_3 support, Pt will dissociate H_2 into H atoms, which react with WO_3 support via the spillover process from blue tungsten to bronze and give electrons to the conduction band of WO_3,

dx.doi.org/10.1021/am505127g | ACS Appl. Mater. Interfaces 2014, 6, 22051−22060

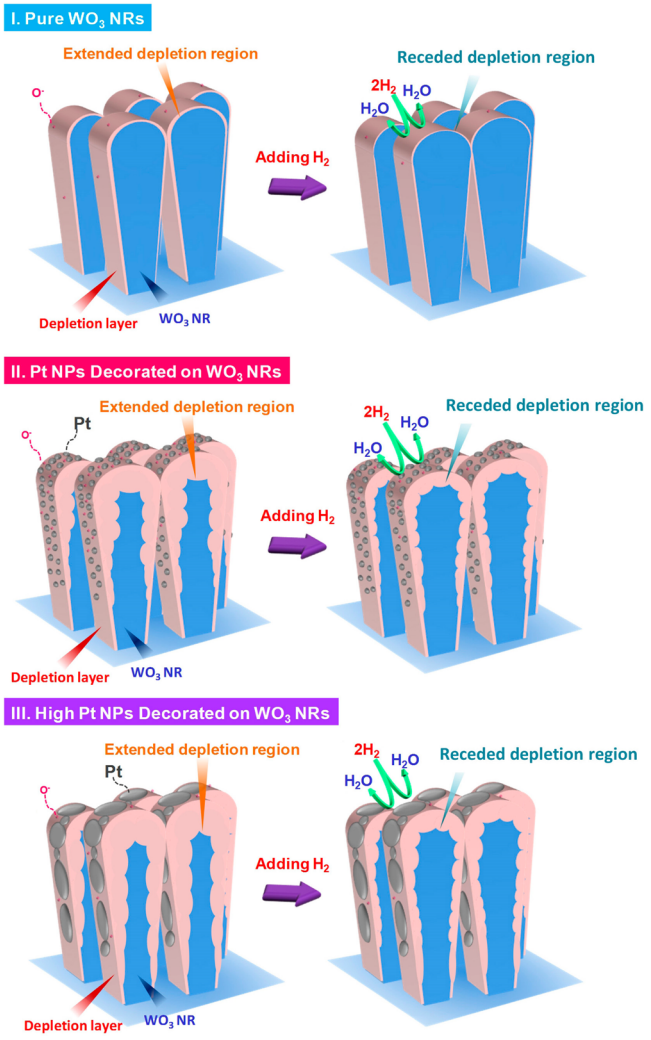

Figure 10. Physical models of gas-sensing mechanisms for (I) undecorated, (II) optimally decorated, and (III) excessively decorated WO_3 nanorods.

resulting in a decrease of depletion width and electrical resistance. Nevertheless, the effectiveness of the spillover mechanism is largely dependent on the structure of support material as well as size, density, and distribution of the Pt sensitizers.

From the characterization results, the size and density of Pt particles decorated on WO_3 nanorods are simultaneously increased as the Pt decoration time increases from 2.5 to 10 s when the H_2 response increases drastically to reach an optimal point at 10 s Pt decoration time. At the optimal Pt concentration, Pt nanoparticles with moderate sizes (~8−30 nm in diameter) and high density are uniformly distributed on WO_3 nanorods as depicted in Figure 10II. In addition, Pt nanoparticles are assumed to penetrate down into WO_3 nanorods as suggested by PES, EDS, and SEM characterization. At thermal equilibrium in air, Pt nanoparticles and WO_3 nanorods form Schottky metal−semiconductor junctions,[22−25] in which Pt nanoparticles with a higher work function acted as electron acceptors extracting an electron from WO_3 nanorods and resulting in extended depletion regions in addition to those formed by oxygen species (see Figure 10I and 10II). As a result, the resistance of the WO_3 nanorod film is increased with increasing Pt decoration time due to increasing size and density of Pt nanoparticles as previously observed from the SEM images in Figure 3. Upon H_2 exposure, H_2 is dissociated by Pt into H atoms that spillover onto WO_3 and react with O^- to produce H_2O and electrons, leading to significant retraction of depletion regions and reduction of resistance.[24−28] With short Pt decoration time (2.5−5 s), Pt nanoparticles begin to enhance the H_2 response via the spillover process but the effect is still relatively low since Pt nanoparticles are very small and mainly cover the very top part of nanorods so that spillover species still do not take much control over the film resistance. At the optimal Pt decoration time (10 s), the density of Pt nanoparticles is sufficiently high so that Pt nanoparticles can cover most inter-rod contacts. Thus, the spillover mechanism becomes highly effective in controlling the resistance of WO_3 nanorods. Moreover, the spillover efficiency may additionally be enhanced due to the increasing contribution of metallic Pt species (Pt^0) from 50% to 60% as Pt decoration time increases from 2.5 to 10 s (see PES result in Figure 6c). Unoxidized Pt^0 has been indicated to play a main role on hydrogen dissociation via an exchange reaction and hydrogen spillover on metal oxide support,[38,39] while Pt species bounded at high oxidation states are much less reactive. Nevertheless, the change in Pt oxidation state of decorated Pt nanoparticles is rather small and its contribution on the enhanced H_2 response should not be substantial.

When the Pt decoration time further increases to 15 s, the size of Pt nanoparticles is increased but its density is decreased due to agglomeration. The coalescence of Pt atoms into large particles leads to lower particle density and reduced Pt−WO_3 interfacial regions where spillover species can interact as depicted in Figure 10III. In addition, the surface area of WO_3 nanorods exposed to air and the number of oxygen species on WO_3 surface to react with spillover species are also reduced. Thus, the spillover effect becomes less effective and H_2 response is deteriorated. Moreover, the coalescence leads to reduced resistance paths through surface conduction along partially connected Pt particles as depicted in the model (Figure 10III) and observed from SEM images (Figure 3). Moreover, the baseline resistance of Pt-decorated WO_3 nanorods with a 15 s Pt decoration time turns to be lower than that with 10 s Pt decoration time despite the fact that larger Pt particles will induce larger depletion regions in WO_3 nanorods. The short resistance paths due to a high Pt loading level contributes significantly to the degraded H_2 response since conduction through them is not affected by gas interaction.

The effectiveness of the spillover mechanism also depends considerably on the structure of the supporting metal oxide material. Table 1 compares the H_2-sensing performance of Pt-decorated WO_3 nanorods with those of other Pt/WO_3 structures reported previously.[22−28] It is evident that the responses of Pt-decorated WO_3 nanorods (1600 to 150 ppm of H_2 and 2.2×10^5 to 3000 ppm of H_2) are much higher than those of other thin-film-based Pt/WO_3 structures including Pt thin film/WO_3 thin film, Pt/WO_3 composite thin film, and Pt nanoparticles/WO_3 thin films prepared by different methods (0.02−26.5 to 200 ppm of H_2 and 250 to 3000 ppm of H_2). Moreover, the Pt-decorated WO_3 nanorod sensor exhibits better performance than a highly sensitive Pt/WO_3 nanoparticle sensor made by flame spray pyrolysis, which displayed the highest response of 2.2×10^4 to 3000 ppm of H_2 at 150 °C.[28] Therefore, the H_2 response of the Pt/WO_3 sensor is highly dependent on morphological structure and preparation method of the WO_3 support and Pt catalyst. In addition,

Table 1. Hydrogen-Sensing Performances of Various Pt/WO_3 Structures Prepared by Different Methods

structure	method	H_2 concentration	loading	response
WO_3 thin film[18]	reactive magnetron sputtering	1000 ppm	unloaded WO_3	response ≈ 13.6 to 1000 ppm at 300 °C
Pt thin film/WO_3 thin film[22]	radiofrequency (rf) reactive sputtering and evaporation	500 ppm	uncoated	response ≈ 0.01 at 250 °C
			Pt coated	response ≈ 0.02 at 150 °C
Pt nanoparticles/WO_3 thin film[23]	rf and dc magnetron sputtering	1250–10000 ppm	unloaded WO_3	response ≈ 9 to 10 000 ppm of H_2 at 150 °C
			Pt-loaded WO_3	response ≈ 1600 to 10 000 ppm of H_2 and ~250 to 3000 ppm of H_2 at 70 °C
Pt/WO_3 composite thin film[24]	R.F. Sputtering with composite target followed by two-step heat treatment.	30–200 ppm	0.5 atom % Pt/WO_3	response ≈ 27 at 95 °C and ~9.5 at 95 °C to 200 ppm of H_2
Pt/WO_3 composite thin film[25]	rf sputtering with composite target	25–200 ppm	1.0 atom % Pt/WO_3	response ≈ 15 to 100 ppm at 100 °C
Pt nanoparticles/WO_3 thin film[26]	dc sputtering and dip coating	50–200 ppm	1.0 atom % Pt/WO_3	response ≈ 25.6 to 200 ppm at 150 °C
Pt nanoparticles/WO_3 thin film[27]	rf magnetron sputtering and electroless plating	50–200 ppm	Pt decorated	response ≈ 7.5–200 ppm at 150 °C
Pt/WO_3 nanoparticles[28]	flame spray pyrolysis/spin-coating	100–10000 ppm	1.0 wt % Pt-loaded WO_3	response ≈ 1.34×10^5 to 10 000 ppm at 150 °C
				response ≈ 2.2×10^4 to 3000 ppm at 150 °C
Pt/WO_3 nanorods (this work)	sputtering with GLAD	150–3000 ppm	Pt-decorated WO_3	response ≈ 2.2×10^5 to 3000 ppm and ~1600 to 150 ppm at 150–200 °C

nanoporous structures of WO_3 supports including nanoparticles and particularly vertically aligned nanorods are highly beneficial for chemical sensitization via the spillover mechanism. The porous and high surface-to-volume ratio structure allows a high-density and uniform distribution of Pt-sensitizing nanoparticles, which efficiently generate and distribute spillover hydrogen species on WO_3 surfaces. Furthermore, the results demonstrate that vertically aligned WO_3 nanorods are even more effective supports than WO_3 nanoparticles. The reason for the superior performance may be attributed to the fact that the WO_3 nanorods are not prone to agglomeration like WO_3 nanoparticles. On the basis of the observed importance of supporting nanostructure, the performance of Pt-decorated WO_3 nanostructured sensors should be further optimized by varying various GLAD conditions, and the results may be presented elsewhere. It should be noted that the WO_3 nanorod structure could not be first optimized for H_2 sensing before Pt decoration because undecorated WO_3 nanorods exhibited a negligible H_2 response so that the influence of WO_3 nanorod morphology on H_2 sensing could not be determined. Thus, optimization of WO_3 nanorods structure for H_2 sensing should be done together with Pt decoration. Nevertheless, the condition used for the WO_3 nanorod deposition has been systematically optimized for structural morphology with small rod size and large inter-rod spacing based on the results of previous studies,[19,20,31,32] and the resulting H_2-sensing performance is outstanding compared with those in most other reports.

Regarding the temperature-dependence characteristics, Pt-decorated WO_3 nanorods exhibit optimum hydrogen response at low temperatures of 150–200 °C and the response drastically decreases with increasing operating temperature. The result is similar to several Pt/WO_3 sensors prepared by different methods.[25−28] A possible explanation for the negative temperature dependence of H_2 response is that the hydrogen dissociation efficiency of Pt will be substantially hindered by the increased density of oxygen species (i.e., O^-) adsorbed around Pt nanoparticles at a high temperature (250–350 °C).[28] Adsorption of oxygen species on the Pt surface will oxidize metallic Pt^0 into Pt species with higher oxidation states and largely shield Pt from hydrogen molecules, diminishing hydrogen dissociation and the spillover effect of Pt nanoparticles. The density of Pt^0 is rapidly and monotonically decreased as the temperature increases from 200 to 350 °C due to thermally activated oxygen species. As a result, the spillover process by Pt nanoparticles becomes less effective and hydrogen response decreases with increasing operating temperature from 200 to 350 °C.

4. CONCLUSIONS

New hydrogen gas sensors have been successfully developed by decoration of sputtered Pt nanoparticles on vertically aligned WO_3 nanorods fabricated via dc magnetron sputtering with the GLAD technique. Pt nanoparticles were sputtered on the WO_3 nanorod surfaces with varying times from 2.5 to 15 s and annealed in air at 400 °C. The size and density of Pt particles decorated on WO_3 nanorods are simultaneously increased as the Pt decoration time increases from 2.5 to 10 s when the H_2 response increases drastically to reach an optimal point at 10 s Pt decoration time. The optimal Pt-decorated WO_3 nanorod sensor exhibits an exceptionally high response of 2.2×10^5 to 3000 ppm of H_2 at 200 °C. In addition, it can sensitively detect low H_2 concentration of less than 150 ppm at a low operating temperature of 150 °C. Moreover, sensor response is rapidly

decreased while the response time is slightly reduced with increasing operating temperature. The excellent H_2-sensing performance may be attributed to highly efficient chemical sensitization by high-density Pt nanoparticles on highly porous crystalline WO_3 nanorods. Therefore, WO_3 nanorods prepared by GLAD with the optimal decoration of Pt nanoparticles are highly potential for hydrogen-sensing applications.

AUTHOR INFORMATION

Corresponding Author

*Tel.: +66-2564-5600. E-mail: mati.horprathum@nectec.or.th.

Author Contributions

M. Horprathum, A. Wisitsirrat, S. Porntheeraphat, and P. Chindaudom designed this experiment, and M. Horprathum prepared the manuscript. Experiments were carried out by M. Horprathum, T. Srichaiyaperk, B. Samransuksamer, P. Eiamchai, S. Limwichean, C. Chananonnawathorn, C. Oros, V. Patthanasettakul, H. Nakajima, and M. Horprathum. A. Wisitsirrat, K. Aiempanakit, N. Nuntawong, S. Porntheeraphat, P. Songsiriritthigul, A. Tuantranont, and P. Chindaudom have analyzed the results and discussed the manuscript during preparation. All authors discussed the results and implications and commented on the manuscript at all stages.

Notes

The authors declare no competing financial interest.

ACKNOWLEDGMENTS

This work was supported by National Electronics and Computer Technology Center, National Science and Technology Development Agency (NSTDA), Thailand.

REFERENCES

(1) Wongchoosuk, C.; Wisitsoraat, A.; Phokharatkul, D.; Tuantranount, A.; Kerdcharoen, T. Multi-Walled Carbon Nanotube-Doped Tungsten Oxide Thin Films for Hydrogen Gas Sensing. *Sensors* **2010**, *10*, 7705−7715.

(2) Gu, H.; Wang, Z.; Hu, Y. Hydrogen Gas Sensors Based on Semiconductor Oxide Nanostructure. *Sensors* **2012**, *12*, 5517−5550.

(3) Chan, C. C.; Hsu, W. C.; Chang, C. C.; Hsu, C. S. Preparation and Characterization of Gasochromic Pt/WO_3 Hydrogen Sensor by Using the Taguchi Design Method. *Sens. Actuators B* **2010**, *145*, 691−697.

(4) Zhang, M.; Yuan, Z.; Song, J.; Zheng, C. Improvement and Mechanism for the Fast Response of a Pt/TiO_2 Gas Sensor. *Sens. Actuators B* **2010**, *148*, 87−92.

(5) Steinebach, H.; Kannan, S.; Rieth, L.; Solzbacher, F. H_2 Gas Sensor Performance of NiO at High Temperatures in Gas Mixtures. *Sens. Actuators B* **2010**, *151*, 162−168.

(6) Yoo, K. S.; Park, S. H.; Kang, J. H. Nano-Grained Thin-Film Indium Tin Oxide Gas Sensors for H_2 Detection. *Sens. Actuators B* **2005**, *108*, 159−164.

(7) Huotari, J.; Lappalainen, J.; Puustinen, J.; Lloyd Spetz, A. Gas Sensing Properties of Pulsed Laser Deposited Vanadium Oxide Thin Films with Various Crystal Structures. *Sens. Actuators B* **2013**, *187*, 386−394.

(8) Dabbous, S.; Ben Nasrallah, T.; Ouerfelli, J.; Boubaker, K.; Amlouk, M.; Belgacem, S. Study of Structural and Optical Properties of Sprayed WO_3 Thin Films using Enhanced Characterization Techniques Along with the Boubaker Polynomials Expansion Scheme (BPES). *J. Alloys Compd.* **2009**, *487*, 286−292.

(9) Horprathum, M.; Limwichean, K.; Wisitsoraat, A.; Eiamchai, P.; Aiempanakit, K.; Limnonthakul, P.; Nuntawong, N.; Pattantsetakul, V.; Tuantranont, A.; Chindaudom, P. NO_2-Sensing Properties of WO_3 Nanorods Prepared by Glancing Angle DC Magnetron Sputtering. *Sens. Actuators B* **2013**, *176*, 685−691.

(10) Wongchoosuk, C.; Wisitsoraat, A.; Phokharatkul, D.; Horprathum, M.; Tuantranont, A.; Kerdcharoen, T. Carbon Doped Tungsten Oxide Nanorods NO_2 Sensor Prepared by Glancing Angle RF Sputtering. *Sens. Actuators B* **2013**, *181*, 388−394.

(11) Bendahan, M.; Boulmani, R.; Seguin, J. L.; Aguir, K. Characterization of Ozone Sensors Based on WO_3 Reactively Sputtered Films: Influence of O_2 Concentration in The Sputtering Gas, and Working Temperature. *Sens. Actuators B* **2004**, *100*, 320−324.

(12) Hieu, N. V.; Quang, V. V.; Hoa, N. D.; Kim, D. Preparing Large-Scale WO_3 Nanowire-Like Structure for High Sensitivity NH_3 Gas Sensor Through a Simple Route. *Curr. Appl. Phys.* **2011**, *11*, 657−661.

(13) Davazoglou, D.; Dritsas, T. Fabrication and Calibration of a Gas Sensor Based on Chemically Vapor Deposited WO_3 Films on Silicon Substrates: Application to H_2 Sensing. *Sens. Actuators B* **2001**, *77*, 359−362.

(14) Siciliano, T.; Tepore, A.; Micocci, G.; Serra, A.; Manno, D.; Filippo, E. WO_3 Gas Sensors Prepared by Thermal Oxidization of Tungsten. *Sens. Actuators B* **2008**, *133*, 321−326.

(15) Wang, L.; Teleki, A.; Pratsinis, S. E.; Gouma, P. I. Ferroelectric WO_3 Nanoparticles for Acetone Selective Detection. *Chem. Mater.* **2008**, *20*, 4794−4796.

(16) White, C. M.; Gillaspie; Dane, T.; Whitney, E.; Lee, S.-H.; C. Dillon, A. Flexible Electrochromic Devices Based on Crystalline WO_3 Nanostructures Produced with Hot-Wire Chemical Vapor Deposition. *Thin Solid Films* **2009**, *517*, 3596−3599.

(17) Li, Y. B.; Bando, Y.; Golberg, D.; Kurashima, K. WO_3 Nanorods/Nanobelts Synthesized via Physical Vapor Deposition Process. *Chem. Phys. Lett.* **2003**, *367*, 214−218.

(18) Shen, Y.; Yamazaki, T.; Liu, Z.; Meng, D.; Kikuta, T.; Nakatani, N. Influence of Effective Surface Area on Gas Sensing Properties of WO_3 Sputtered Thin Films. *Thin Solid Films* **2009**, *517*, 2069−2072.

(19) Deniz, D.; Frankel, D. J.; Lad, R. J. Nanostructured Tungsten and Tungsten Trioxide Films Prepared by Glancing Angle Deposition. *Thin Solid Films* **2010**, *518*, 4095−4099.

(20) Deniz, D.; Lad, R. J. Temperature Threshold for Nanorod Structuring of Metal and Oxide Films Grown by Glancing Angle Deposition. *J. Vac. Sci. Technol. A* **2011**, *29*, 011020.

(21) Hsu, W.-C.; Chan, C.-C.; Peng, C.-H.; Chang, C.-C. Hydrogen Sensing Characteristics of an Electrodeposited WO_3 Thin Film Gasochromic Sensor Activated by Pt Catalyst. *Thin Solid Films* **2007**, *516*, 407−411.

(22) Penza, M.; Martucci, C.; Cassano, G. NO_x Gas Sensing Characteristics of WO_3 Thin Films Activated by Noble metals (Pd, Pt, Au) Layers. *Sens. Actuators B* **1998**, *50*, 52−59.

(23) Ippolito, S. J.; Kandasamy, S.; Kalantar-zadeh, K.; Wlodarski, W. Hydrogen Sensing Characteristics of WO_3 Thin Film Conductometric Sensors Activated by Pt and Au Catalysts. *Sens. Actuators B* **2005**, *108*, 154−158.

(24) Zhang, C.; Boudiba, A.; Navio, C.; Biterncourt, C.; Olivier, M.-G.; Snyders, R.; Debliquy, M. Highly Sensitive Hydrogen Sensors Based on Co-Sputtered Platinum-Activated Tungsten Oxide Films. *Int. J. Hydrogen Energy* **2011**, *36*, 1107−1114.

(25) Zhang, C.; Boudiba, A.; Olivier, M.-G.; Snyders, R.; Debliquy, M. Sensing Properties of Pt/Pd Activated Tungsten Oxide Films Grown by Simultaneous Radio-Frequency Sputtering to Reducing Gases. *Sens. Actuators B* **2012**, *175*, 53−59.

(26) Zhang, C.; Boudiba, A.; Olivier, M.-G.; Snyders, R.; Debliquy, M. Magnetron Sputtered Tungsten Oxide Films Activated by Dip-Coated Platinum for ppm-Level Hydrogen Detection. *Thin Solid Films* **2012**, *520*, 3679−3683.

(27) Zhang, C.; Kanta, A.-F.; Yin, H.; Boudiba, A.; D'Haen, J.; Olivier, M.-G.; Debliquy, M. H_2 Sensors Based on WO_3 Thin Films Activated by Platinum Nanoparticles Synthesized by Electroless Process. *Int. J. Hydrogen Energy* **2013**, *38*, 2929−2935.

(28) Samerjai, T.; Tamaekong, N.; Liewhiran, C.; Wisitsoraat, A.; Tuantranont, A.; Phanichphant, S. Selectivity Towards H_2 Gas by Flame-Made Pt-Loaded WO_3 Sensing Films. *Sens. Actuators B: Chem.* **2011**, *157*, 290−297.

(29) Liu, X.; Zhang, J.; Yang, T.; Guo, X.; Wu, S.; Wang, S. Synthesis of Pt Nanoparticles Functionalized WO_3 Nanorods and Their Gas Sensing Properties. *Sens. Actuators B* **2011**, *156*, 918−923.
(30) Noothongkaew, S.; Nakajima, H.; Tong-On, A.; Meevasana, W.; Songsiriritthigul, P. Oxidation of Zn in UHV Environment at Low Temperature. *Appl. Surf. Sci.* **2012**, *258*, 1955−1957.
(31) Robbie, K.; Brett, M. J. Sculptured Thin Films and Glancing Angle Deposition: Growth Mechanics and Applications. *J. Vac. Sci. Technol. A* **1997**, *15*, 1460−1465.
(32) Zhao, Y.-P.; Ye, D.-X.; Wang, G.-C.; Lu, T.-M. Designing Nanostructures by Glancing Angle Deposition. *SPIE Proc.* **2003**, *5219*, 59−73.
(33) Fedorovich, R. D.; Naumovets, A. G.; Tomchuk, P. M. Electron and Light Emission from Island Metal Films and Generation of Hot Electrons in Nanoparticles. *Phys. Rep.* **2000**, *328*, 73−179.
(34) Jensen, P. Growth of Nanostructures by Cluster Deposition: Experiments and Simple Models. *Rev. Mod. Phys.* **1999**, *71*, 1695−1735.
(35) Klimovskaya, A.; Sarikov, A.; Pedchenko, Y.; Voroshchenko, A.; Lytvyn, O.; Stadnik, A. Study of The Formation Processes of Gold Droplet Arrays on Si Substrates by High Temperature Anneals. *Nanoscale Res. Lett.* **2011**, *6*, 151.
(36) Kim, M.-S.; Lee, D.-W.; Chung, S.-H.; Hong, Y.-K.; Lee, S. H.; Oh, S.-H.; Cho, I.-H.; Lee, K.-Y. Oxidation of Ammonia to Nitrogen over Pt/Fe/ZSM5 Catalyst: Influence of Catalyst Support on the Low Temperature Activity. *J. Hazard. Mater.* **2012**, *237*−*238*, 153−160.
(37) Aricò, A. S.; Shukla, A. K.; Kim, H.; Park, S.; Min, M.; Antonucci, V. An XPS Study on Oxidation States of Pt and Its Alloys with Co and Cr and Its Relevance to Electroreduction of Oxygen. *Appl. Surf. Sci.* **2001**, *172*, 33−40.
(38) Yatsimirskii, V. K.; Lesnyak, V. V.; Gut, I. N.; Boldyreva, O.Yu. Effect of Pt, Pd, and Cs+ additives on the surface state and catalytic activity of WO_3 in oxidation of hydrogen. *Theor. Exp. Chem.* **2005**, *41*, 135−138.
(39) Horiuti, I.; Polanyi, M. Exchange reactions of hydrogen on metallic catalysts. *Trans. Faraday Soc.* **1934**, *30*, 1164−70.